Excited states and electronic spectra of extended tetraazaporphyrins

Ryoichi Fukuda,[1,2,3,a)] Masahiro Ehara,[1,3] and Hiroshi Nakatsuji[2,3]
[1]*Department of Theoretical and Computational Molecular Science, Institute for Molecular Science, 38 Nishigo-Naka, Myodaiji, Okazaki 444-8585, Japan and Research Center for Computational Science, 38 Nishigo-Naka, Myodaiji, Okazaki 444-8585, Japan*
[2]*Quantum Chemistry Research Institute, Kyodai Katsura Venture Plaza, 1-36 Goryo Oohara, Nishikyo-ku, Kyoto 615-8245, Japan*
[3]*Japan Science and Technology Agency, CREST, Sanboncho-5, Chiyoda-ku, Tokyo 102-0075, Japan*

(Received 28 June 2010; accepted 30 August 2010; published online 14 October 2010)

Electronic excited states, electronic absorption, and magnetic circular dichroism (MCD) spectra of free-base tetraazaporphyrin (TAP), phthalocyanine (Pc), naphthalocyanine (Nc), and anthracocyanine (Ac) were studied by quantum chemical calculations using the symmetry-adapted cluster-configuration interaction (SAC-CI) method. Not only optically allowed states including the Q- and B-bands but also optically forbidden states were calculated for transitions whose excitation energies were lower than 4.5 eV. The present SAC-CI calculations consistently assigned the absorption and MCD peaks as optically allowed $\pi \rightarrow \pi^*$ excitations, although these calculations using double-zeta basis limit quantitative agreement and discussion. For Nc and Ac, excited states beyond the four-orbital model appeared in the low-energy region. The low-energy shifts of the Q-bands with the extension of molecular size were explained by the orbital energies. The splitting of the Q-bands decreases with extension of the molecular size. This feature was reproduced by the SAC-CI calculations but the configuration interaction with single excitations and time-dependent density functional theory calculations failed to reproduce this trend. Electron correlation in the excited states is important in reproducing this splitting of the Q-bands and in describing the energy difference between the B_{2u} and B_{3u} states of free-base porphyrins. © *2010 American Institute of Physics*. [doi:10.1063/1.3491026]

I. INTRODUCTION

Electronic excitations of porphyrin congeners are being actively studied because their optical properties are important in physics, chemistry, biology, industry, and many other fields. On the subject of their excited states, porphyrins show characteristic photoabsorption in the near-UV (ultraviolet) and in the visible regions. An intense band, called a B- or Soret band, is observed usually around 3 eV (400 nm) of excitation energy. Several weak absorptions arising from Q-bands are observed usually in the region 2.5–1.8 eV (500–700 nm). Actual absorption energies, intensities, number of bands, and band profiles strongly depend on chemical substitutions and modifications at the β- and mesopositions, and the coordination of metals. Indeed, tuning the absorption characters by chemical techniques is one of the major subjects of porphyrin chemistry. In this study, we focus on rather standard tetraazaporphyrins (TAPs) (also known as porphyrazines) and their congeners that are sequentially extended by addition of fused benzene rings such as phthalocyanine.

TAP is a compound that is derived by the introduction of nitrogen at the four mesopositions of the porphyrin basic skeleton (named as porphin).[1,2] What makes this compound so attractive is the high intensity of its Q-bands. The weak intensity of the Q-bands in unmodified porphin is explained by the cancellation of transition dipole moments between the transition from the highest occupied molecular orbital (HOMO) and the next-HOMO. Replacement at the mesopositions by nitrogen stabilizes the orbital energy of the next-HOMO and breaks the balance between those two transitions.[1,3] Consequently, the Q-bands of TAP in the visible region have high intensity, therefore TAP is regarded as an important fundamental material of dyes and pigments.[1,2] Phthalocyanines (Pc) are important derivatives of TAP that are widely used as chromophores and other materials in many fields.

There have been many theoretical studies on the excited states of porphyrins because of their scientific and practical importance. The fundamental interpretation of the porphin UV-vis spectrum is based on Gouterman's four-orbital model, which explains the Q- and B-bands in terms of electron transitions between the two HOMOs and two lowest unoccupied molecular orbitals (LUMOs).[4] Although the four-orbital model is helpful for qualitative understanding of the spectra and optical properties, *ab initio* calculations are necessary for qualitative predictions of more general porphyrins containing various substituents. Such reliable calculations may elucidate mechanisms of photophysical and photochemical phenomena related to porphyrins. However, there have not been many studies using high-level *ab initio* calculations on excited states of porphyrins because they are large for high-level wave function theories for excited states. For free-base porphin, the excited states calculation using symmetry-adapted cluster-configuration interaction (SAC-

a)Electronic mail: fukuda@ims.ac.jp.

CI) have been first reported.[5] Then the calculations using equation-of-motion coupled-cluster (EOM-CC),[6] complete active-space second-order perturbation theory (CASPT2),[7] and multireference Møller–Plesset theory (MRMP) (Ref. 8) have been reported. Density functional theory (DFT), which is extensively applied to large-scale calculations, seems to still have problems with excited states of such extended systems when using standard functionals.[9]

We studied theoretically the electronic excited states and UV-vis spectra of TAP (Ref. 3) and Pc (Ref. 10) by the SAC-CI method in 1996 and 1997, respectively. In those studies, we analyzed and assigned the peaks of spectra based on the *ab initio* SAC-CI calculations and proposed orbital pictures and mechanisms for the electron transitions. The SAC-CI method considers electron correlation by the cluster expansion and electron excitations are described by the configuration interaction formula as an eigenvalue problem.[11] The method can describe the ground and excited states in compact and well-balanced form; moreover, the theory is size-consistent.[12] Therefore, the method can be safely applied to π-electron excitations in large systems such as porphyrins. To execute practical calculations on large molecules, the SAC-CI program can use a perturbation-selection technique, in which computational dimensions can be reduced by neglecting less important configurations.[13] One can manage the accuracy of the calculations, computer resources, and computational time by setting appropriate selection thresholds. This study can be regarded as one recent progress in those series of SAC-CI studies on TAP, Pc, and other azaporphyrins.[14]

Recently, a series of TAP congeners were synthesized and their UV-vis and magnetic circular dichroism (MCD) spectra were measured by Kobayashi's group.[2,15–18] In particular they studied[16] the properties of TAP, Pc, naphthalocyanine (Nc), and anthracocyanine (Ac) (it is also called anthracyanine); those compounds may be classified as a series of TAP derivatives in which π-systems are extended by the sequential addition of fused benzene rings. They discussed the relations between properties and molecular sizes for free-base (metal free) and some metal compounds. Bathochromic shifts (redshifts) of the Q-bands were observed in accordance with the extension of molecular sizes; however, the degree of the shifts was suppressed. An interesting feature of this series of free-base compounds is that the splitting of the Q-bands decreases with increasing molecular size. As a result, the Q-bands of free-base Nc (H_2Nc) and free-base Ac (H_2Ac) appeared as a single band in the UV-vis spectra, while the splitting was observed for free-base TAP (H_2TAP) and free-base Pc (H_2Pc). In the B-band region, the MCD spectra provided valuable insight into the nature of the broad absorptions by resolving them into positive and negative MCD signals.

The observed trend for the splitting of the Q-bands could not be explained by the Zerner's intermediate neglect of differential overlap (ZINDO) calculation[16] and time-dependent DFT (TDDFT) study,[19] whereas these methods well reproduced the redshifts of the Q-bands.[16,18,19] Kobayashi *et al.* supposed that this splitting of the Q-bands in free-base compounds may be explained by a splitting of the LUMOs.[16] However, this assumption seems to be contradicted by the TDDFT results.[19] Further theoretical studies are required to elucidate the reason for the decrease in the splitting of the Q-bands. These experimental findings then motivated us to study this series of TAP compounds using the SAC-CI method.

In this study, we investigated the electronic excited states of H_2TAP, H_2Pc, H_2Nc, and H_2Ac by *ab initio* quantum chemical calculations using the SAC-CI method. For these compounds we gave assignments for the observed UV-vis and MCD spectra based on the SAC-CI calculations. The deviations were about 0.3 eV between the present SAC-CI with D95 basis calculations and the observed UV-vis/MCD peaks; they seem to be reasonable errors for such large molecules. We showed that the calculation results can be improved by augmentation of the polarization functions if enough computer resources are available. We also calculated optically forbidden states because they are important in designing related molecules and molecular systems.[1,2,20]

It is interesting to compare the nature of the excited states among a series of compounds. To elucidate the correlations of each excited state between a series of compounds is important not only in terms of scientific interests but also for applications in molecular design. For this purpose, excited states were analyzed in terms of the MO character. In H_2Nc and H_2Ac, several low-lying $\pi \rightarrow \pi^*$ excitations that are not covered by the four-orbital model were calculated. For H_2Ac such states were calculated and observed between the Q- and B-bands. These states had been suggested by the ZINDO calculations[16] and the present study is the first *ab initio* calculations for the excited states of Nc and Ac beyond the Q-bands.

The present SAC-CI and perturbative doubles correction for configuration interaction with single excitations [CIS(D)] calculations could explain the experimental trend in the splitting of the Q-bands that could not be explained by the orbital energy levels and CIS. The standard TDDFT calculations failed to reproduce that experimental trend. The long-range correction (LC) (Ref. 21) significantly revised the excitation energies calculated by TDDFT; however, the effect was not enough to explain the experimental findings. The present results suggest that dynamic electron correlation is essential to explain the relative excitation energies of the Q_x- and Q_y-bands for free-base compounds. The energy difference of these two states is caused by the inner hydrogens, which break the D_{4h} point group symmetry and degeneracy of the LUMOs. There are two types of interactions in these states: proton-proton interaction and electron-electron interaction in the lone pairs. Dynamic electron correlation is significant for lone pairs and proton-proton interactions may be described by electrostatic terms. We supposed that accurate excited state theories are necessary to explain those excited states in which several interactions from different characters exist. To our knowledge, the electronic origin of the splitting of the Q-bands has not been studied in detail for free-base porphyrins and phthalocyanines beyond the four-orbital model. This study explicitly shows the limitation of orbital models for studying electronic excitations and interpreting the UV-vis spectra even for qualitative understanding purposes.

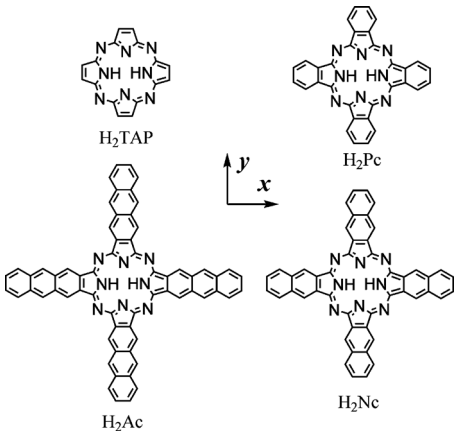

FIG. 1. Molecular formula and coordinate of free-base tetraazaporphyrin (H_2TAP), free-base phthalocyanine (H_2Pc), free-base naphthalocyanine (H_2Nc), and free-base anthracocyanine (H_2Ac).

II. COMPUTATIONAL DETAILS

The molecular geometries were optimized by the Becke three-parameter exchange and Lee–Yang–Parr correlation[22] (B3LYP) DFT calculation with the 6-31G* basis set.[23] During the optimization, the geometry was constrained to the D_{2h} point group symmetry. The optimized structures have no negative vibrational frequencies; therefore the planar D_{2h} structure is a local minimum. The molecular structure and coordinates in this study are shown in Fig. 1; the protonated pyrroles are put on the *x*-direction and the others are put on the *y*-direction.

The SAC/SAC-CI calculations were performed with the latest direct SAC-CI program[24] combined with the GAUSSIAN development version.[25] The D95 basis set[26] was used, except where noted otherwise. The 1s electrons of C and N atoms were excluded for the SAC and SAC-CI calculations as the frozen-core approximation. The perturbation-selection technique was used for the SAC/SAC-CI calculation: the double excitation operators whose second-order contribution to the energy is less than the given threshold are neglected.[13] The selection thresholds for the ground and the excited states were 2.0×10^{-7} and 2.0×10^{-8}, respectively; they are the limits of the present computer resource. The number of basis functions, active molecular orbitals (MOs), and selected SAC/SAC-CI dimensions are summarized in Table I.

For the present calculations, SAC-CI eigenvectors and eigenvalues were calculated by an iterative method using CIS results as initial guesses; therefore, the present results contain only the states of single electron excitation with respect to the closed-shell configuration. Low-lying double electron excited states may exist, which have main configurations of two-electron excitation from the closed-shell Hartree–Fock state such as the $1\,^1A_{1g}$ state of trans polyenes[27] and polyacens.[28] Such states are optically forbidden and not important for UV-vis spectra. Although such dark states may be important for applications to electronic materials and molecular devices,[29] we do not discuss them in the present paper.

To compare with the SAC/SAC-CI results, we also performed the CIS, CIS(D) (Ref. 30), and TDDFT calculations using the same computational conditions as those of the SAC/SAC-CI. For the TDDFT calculations, we used the B3LYP functional. We also performed BLYP and LC-BLYP calculations to investigate the effect of the long-range correction that could be significant for $\pi\rightarrow\pi^*$ excitations of large systems.[21]

The CIS and CIS(D) calculations were performed using GAUSSIAN09 (Ref. 31) and the TDDFT calculations were performed using the GAMESS program.[32] In this paper, we will discuss excitation energies using eV unit although experimental spectra have been reported in nm because it is convenient to discuss the accuracy of different systems on the

TABLE I. The number of basis functions for the Hartree–Fock calculations, the number of active orbitals, and the dimensions for the SAC/SAC-CI calculations.

	H_2TAP		H_2Pc		H_2Nc		H_2Ac	
Formula	$C_{16}H_{10}N_8$		$C_{32}H_{18}N_8$		$C_{48}H_{26}N_8$		$C_{64}H_{34}N_8$	
Basis[a]	236		396		556		716	
Occ./unocc.[b]	57/155		93/263		129/371		165/479	
Dimensions	Sel./full[c]	N[d]	Sel./full[c]	N[d]	Sel./full[c]	N[d]	Sel./full[c]	N[d]
X ^1A_g [e]	1 316 502/5 318 465	1	3 006 080/40 824 313	1	4 095 489/156 427 585	1	4 601 814/426 806 873	1
^1A_g	391 926/5 318 465	3	1 263 205/40 824 013	3	2 220 484/156 427 585	4	3 348 815/426 806 873	7
$^1B_{1g}$	327 378/5 313 876	2	876 689/40 811 968	2	2 269 721/156 403 436	5	3 328 791/426 766 488	6
$^1B_{2g}$	408 849/4 445 476	2	968 133/33 974 472	2	1 429 462/129 918 884	2	2 306 248/354 069 112	3
$^1B_{3g}$	443 971/4 445 324	2	1 061 800/33 974 376	2	1 501 626/129 918 924	2	2 268 371/354 069 368	3
^1A_u	414 898/4 445 316	2	909 739/33 974 376	2	1 355 745/129 918 868	2	2 270 134/354 069 144	3
$^1B_{1u}$	503 909/4 445 484	3	1 205 419/33 974 482	3	1 688 085/129 918 940	3	1 917 496/354 069 336	3
$^1B_{2u}$	522 511/5 313 884	5	1 300 077/4 081 1984	5	2 841 484/156 403 636	7	3 987 357/426 767 288	9
$^1B_{3u}$	546 035/5 314 040	5	1 397 845/4 081 2068	5	2 760 252/156 403 456	7	3 948 567/426 766 556	9

[a]The number of basis functions.
[b]The number of occupied/unoccupied active orbitals.
[c]The selected/full dimensions of the SAC and SAC-CI calculations.
[d]The number of reference CIS states for the perturbation-selection.
[e]The SAC ground state.

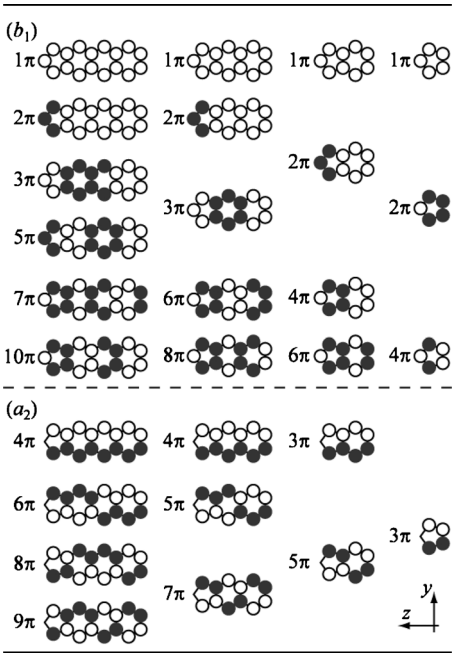

FIG. 2. The nodal structures of the π-orbitals of pyrrole and isoindole congeners. For each molecule, the largest number orbitals are unoccupied and the others are occupied.

energy scale rather than the wavelength scale. In this study we consider only singlet excited states; therefore, the notation of spin states will be omitted throughout this paper.

III. MOLECULAR ORBITALS

We analyzed the valence π-orbitals into the orbitals of its constituent ring compounds, pyrroles, or isoindole congeners, for the purpose of explaining the characteristics of these orbitals, and elucidating the orbital correlations between the target TAP derivatives. The nodal structures of the π-orbitals of pyrrole and isoindole congeners are illustrated in Fig. 2. These molecules have C_{2v} point group symmetry and thus the π-orbitals belong to the b_1 or a_2 representations. The a_2 orbitals are antisymmetric for the x-z plane including nitrogen atom. We numbered the π-orbitals by the orbital energy order from the lowest orbital. The highest energy orbitals in Fig. 2 of each molecule are unoccupied.

Table II shows a summary of valence MOs for H_2Ac, H_2Nc, H_2Pc, and H_2TAP, where the irreducible representations, Hartee–Fock orbital energies, and orbital characters are given. The orbitals are categorized into nonbonding (n) orbitals and π-orbitals. The n-orbitals belong to the a_g, b_{1g}, b_{2u}, or b_{3u} representations. They have characters of basically a lone pair of mesonitrogens, pyrrole-nitrogens, or their combinations. The π-orbitals belong to the a_u, b_{1u}, b_{2g}, or b_{3g} representations. They are approximately composed from a linear combination of π-orbitals of mesonitrogen and pyrrole or isoindole congeners. Because of the bond formations in making a macrocyclic molecule, porphyrins' MOs cannot be decomposed simply into a few pyrrole MOs. Here, we intend to study the nature of the excited states and to explain the correlation of peaks between the target TAP derivative compounds; therefore, only qualitative overviews of orbital character are necessary. These are rather helpful in analyzing and understanding the computational results and experimental spectra. Selected MOs of main transitions in Q-band states are shown in Figs. 3–6, where the contour value of the isosurfaces is 0.02.

The HOMO, LUMO, and next-LUMO of these compounds are a_u, b_{2g}, and b_{3g} orbitals with similar characters. The b_{2g} orbitals have a nodal plane in the y-z plane and the b_{3g} orbitals have a nodal plane in the x-z plane. The orbital energy levels of these orbitals are shown in Fig. 7. Extension of the molecular size significantly destabilizes the HOMO but the effects are suppressed in larger systems. Extension of the molecule also destabilizes the b_{3g} next-LUMO level; however, the effect is much smaller than those for the HOMO. The energy levels of the b_{2g} LUMOs are hardly affected by the molecular size.

IV. UV-VISIBLE SPECTRA

The SAC-CI results of H_2TAP, H_2Pc, H_2Nc, and H_2Ac are summarized in Tables III and IV, respectively, where the main configurations of the SAC-CI wave functions, excitation energies, and oscillator strengths are shown with the experimental excitation energies. We show the peak-top positions of the UV-vis absorption spectrum and MCD signals with their signs. The comparisons of the absorption spectrum and SAC-CI results are shown in Fig. 8 where vertical lines show the SAC-CI results. In Fig. 8, we converted the horizontal axis of the spectra of Ref. 16 into the energy scale from wavelengths. The absorption and MCD spectra in Ref. 16 were measured in pyridine solution for the TAP compounds with *tert*-butyl groups at their periphery positions. The present calculations did not include *tert*-butyl groups and solvent effect. A computational method for MCD rotational strengths using the SAC-CI wave function has not been implemented yet. Therefore, we do not discuss the sign of the MCD signals.

Porphyrins with D_{2h} point group symmetry in the coordinates of Fig. 1 have optically allowed $\pi \rightarrow \pi^*$ excitations of B_{2u} and B_{3u} representations whose directions of dipole transition are the y- and x-axes, respectively. The optically allowed $n \rightarrow \pi^*$ transitions have B_{1u} representation. Optically forbidden states were also calculated. They may be unnecessary for assignment of spectra; however, they may play a role for other properties and can be important for molecular design.

A. H_2TAP

Table III shows the experimental results of H_2TAP both with[16] and without[33] *tert*-butyl groups. One can confirm that the effect of *tert*-butyl groups is negligible. The experimental absorptions of the Q-bands were observed at 2.00 and 2.25 eV; they showed positive and negative MCD signals of the Faraday B-terms. The shoulder of the B-band was observed at around 3.5 eV. A small negative absorption was also observed in this region by MCD. The peak top of the B-band was 3.71 eV in the absorption spectrum. The MCD spectrum showed the pseudo-Faraday A-terms (closely lying Faraday B-terms of opposite sign) at 3.60 and 3.91 eV of, respectively, negative and positive signals.

TABLE II. Valence molecular orbitals of H_2Ac, H_2Nc, H_2Pc, and H_2TAP.

H_2Ac				H_2Nc				H_2Pc				H_2TAP			
No.	Rep.[a]	ε[b] (eV)	Character[c]	No.	Rep.	ε (eV)	Character	No.	Rep.	ε (eV)	Character	No.	Rep.	ε (eV)	Character
Higher occupied orbitals															
208	$55a_g$	−12.86	n[N(meso)]	160	$43a_g$	−12.95	n[N(meso)]	116	$31a_g$	−13.11	n[N(meso)]	68	$19a_g$	−13.37	n[N(meso)]
209	$49b_{2u}$	−12.73	n[N(meso),N(py)]	161	$38b_{2u}$	−12.81	n[N(meso),N(py)]	117	$27b_{2u}$	−12.95	n[N(meso),N(py)]	69	$16b_{2u}$	−13.21	n[N(meso), N(py)]
212	$56a_g$	−12.03	n[N(py)]	166	$44a_g$	−12.08	n[N(py)]	119	$32a_g$	−12.16	n[N(py)]	70	$20a_g$	−12.37	n[N(py)]
213	$50b_{3u}$	−11.91	n[N(meso)]	167	$39b_{3u}$	−11.99	n[N(meso)]	120	$28b_{3u}$	−12.11	n[N(meso)]	71	$17b_{3u}$	−12.34	n[N(meso)]
210	$4b_{2g}$	−12.35	π[3π(x),4π(y) +meso]	163	$3b_{2g}$	−12.61	π[2π(x),4π(y) +meso]								
								118	$3b_{2g}$	−12.32	π[2π(x),3π(y) +meso]	72	$2b_{2g}$	−12.25	π[1π(x),3π(y) +meso]
217	$5b_{2g}$	−11.51	π[5π(x) +meso]	165	$4b_{2g}$	−12.21	π[3π(x),4π(y) +meso]								
211	$4b_{3g}$	−12.29	π[4π(x) +meso,3π(y)]	162	$3b_{3g}$	−12.70	π[4π(x) +meso,2π(y)]								
								121	$3b_{3g}$	−12.00	π[3π(x)+meso, 2π(y)]	73	$2b_{3g}$	−12.18	π[3π(x)+meso, 1π(y)]
223	$6b_{3g}$	−10.92	π[5π(y)+meso]	170	$4b_{3g}$	−11.65	π[4π(x) +meso,3π(y)]								
214	$50b_{1u}$	−11.65	n[N(meso),N(py)]	169	$39b_{2u}$	−11.71	n[N(meso),N(py)]	122	$28b_{2u}$	−11.81	n[N(meso),N(py)]	74	$17b_{2u}$	−12.02	n[N(meso),N(py)]
220	$44b_{1g}$	−11.35	n[N(meso)]	171	$34b_{1g}$	−11.43	n[N(meso)]	123	$24b_{1g}$	−11.55	n[N(meso)]	75	$14b_{1g}$	−11.80	n[N(meso)]
216	$7b_{1u}$	−11.53	π[5π(x)]	164	$5b_{1u}$	−12.45	π[3π(x)]								
								125	$5b_{1u}$	−10.12	π[4π(x)+meso]	76	$2b_{1u}$	−11.09	π[2π(x)+meso]
228	$9b_{1u}$	−9.52	π[7π(x)+meso]	176	$7b_{1u}$	−9.73	π[6π(x)+meso]								
229	$8b_{2g}$	−8.95	π[7π(x)]	177	$6b_{2g}$	−9.27	π[6π(x)]	126	$4b_{2g}$	−9.84	π[4π(x)]	77	$3b_{2g}$	−10.96	π[2π(x)]
218	$5b_{3g}$	−11.42	π[6π(x)+meso]												
				174	$5b_{3g}$	−10.74	π[5π(x)+meso]								
226	$7b_{3g}$	−9.68	π[8π(x)+meso]					127	$4b_{3g}$	−9.57	π[5π(x)+meso]				
234	$9b_{3g}$	−7.31	π[9π(x)+meso]	182	$7b_{3g}$	−8.18	π[7π(x)+meso]								
219	$3a_u$	−11.36	π[6π(x) +meso,6π(y)]	173	$3a_u$	−10.83	π[5π(x) +meso,5π(y)]	128	$3a_u$	−9.53	π[5π(x) +meso,5π(y)]				
225	$5a_u$	−9.69	π[8π(x) +meso,8π(y)]												
				184	$5a_u$	−8.08	π[7π(x) +meso,7π(y)]								
236	$7a_u$	−7.19	π[9π(x) +meso,9π(y)]												
221	$6b_{2g}$	−11.25	π[6π(y)+meso]												
				175	$5b_{2g}$	−10.70	π[5π(y)+meso]								
227	$7b_{2g}$	−9.63	π[8π(y)+meso]					129	$5b_{2g}$	−9.40	π[5π(y)+meso]				
235	$9b_{2g}$	−7.23	π[9π(y)+meso]	183	$7b_{2g}$	−8.09	π[7π(y)+meso]								
222	$8b_{1u}$	−11.15	π[5π(y)]	168	$6b_{1u}$	−11.98	π[3π(y)+meso]								
								130	$6b_{1u}$	−9.26	π[4π(y)+meso]	78	$3b_{1u}$	−10.19	π[2π(y)+meso]
230	$10b_{1u}$	−8.71	π[7π(x),7π(y) +meso]	178	$8b_{1u}$	−8.89	π[6π(x),6π(y) −meso]								
231	$8b_{3g}$	−8.64	π[7π(y)]	180	$6b_{3g}$	−8.85	π[6π(y)]	131	$5b_{3g}$	−9.20	π[4π(y)]	79	$3b_{3g}$	−10.08	π[2π(y)]
232	$11b_{1u}$	−8.64	π[7π(x)+meso]	181	$9b_{1u}$	−8.81	π[6π(x) −meso,6π(y)]	132	$7b_{1u}$	−8.97	π[6π(x)+meso]	80	$4b_{1u}$	−9.09	π[4π(x)+meso, 4π(y)]
215	$2a_u$	−11.58	π[4π(x)]	172	$2a_u$	−11.19	π[4π(x),4π(y)]								
								124	$2a_u$	−10.27	π[3π(x),3π(y)]				
224	$4a_u$	−10.15	π[6π(x),6π(y)]	179	$4a_u$	−8.88	π[5π(x),5π(y)]					81	$2a_u$	−6.88	π[3π(x),3π(y)]
233	$6a_u$	−7.91	π[8π(x),8π(y)]												
				185	$6a_u$	−5.09	π[7π(x),7π(y)]	133	$4a_u$	−5.70	π[5π(x),5π(y)]				
237	$8a_u$	−4.75	π[9π(x),9π(y)]												
Lower unoccupied orbitals															
239	$10b_{3g}$	−0.22	π[9π(x)−meso]	187	$8b_{3g}$	−0.32	π[7π(x)−meso]	135	$6b_{3g}$	−0.51	π[5π(x)−meso]	82	$4b_{3g}$	−0.95	π[3π(x),4π(y) +meso]
238	$10b_{2g}$	−0.67	π[9π(y)−meso]	186	$8b_{2g}$	−0.68	π[7π(y)−meso]	134	$6b_{2g}$	−0.73	π[5π(y) −meso]	83	$4b_{2g}$	−0.90	π[4π(x) +meso,3π(y)]

TABLE II. (*Continued.*)

H_2Ac				H_2Nc				H_2Pc				H_2TAP			
No.	Rep.[a]	ε[b] (eV)	Character[c]	No.	Rep.	ε (eV)	Character	No.	Rep.	ε (eV)	Character	No.	Rep.	ε (eV)	Character
244	$9a_u$	2.09	π[9π(x)−meso, 9π(y)]	192	$7a_u$	2.10	π[7π(x)−meso, 7π(y)]	136	$5a_u$	2.11	π[5π(x)−meso, 5π(y)]	84	$3a_u$	2.01	π[3π(x)−meso, 3π(y)]
240	$12b_{1u}$	0.79	π[10π(x)]	188	$10b_{1u}$	1.45	π[8π(x)]	137	$8b_{1u}$	2.40	π[6π(x),6π(y)]	85	$5b_{1u}$	4.45	π[4π(x),4π(y) +meso]
242	$11b_{2g}$	1.11	π[10π(x) −meso]	189	$9b_{2g}$	1.79	π[8π(x) −meso]	138	$7b_{2g}$	2.72	π[6π(x) −meso]				
241	$13b_{1u}$	1.09	π[10π(x)]	190	$11b_{1u}$	1.85	π[8π(y)]	139	$9b_{1u}$	2.88	π[6π(x),6π(y)]				
243	$11b_{3g}$	1.22	π[10π(y) −meso]	191	$9b_{3g}$	1.94	π[8π(y) −meso]	140	$7b_{3g}$	2.92	π[6π(y) −meso]				

[a]Irreducible representation of orbitals.
[b]Hartree–Fock orbital energies.
[c]The orbital characters where π(x) and π(y) denote π-orbitals of pyrrole derivatives on the *x*- and *y*-axes, respectively, and N(meso) and N(py) denote the nitrogen of the mesoposition and pyrrole derivatives, respectively.

For H_2TAP, 18 states were calculated with excitation energies lower than 4.5 eV using the SAC-CI method; they include six optically allowed $\pi \rightarrow \pi^*$ states. The $1B_{3u}$ and $1B_{2u}$ states obviously correspond to the Q_x- and Q_y-bands. The next absorption at around 3.5 eV may be assigned to the $2B_{3u}$ state. Then, the MCD peaks at 3.60 and 3.91 eV have to be assigned to the $2B_{2u}$ and $3B_{2u}$ states, respectively. According to this assignment, the calculated excitation energies of B_{2u} states were overestimated by approximately 0.3 eV in comparison with experiment. This deviation seems to be too large for the purpose of providing a reliable assignment. We additionally performed the SAC-CI calculation using the D95 (d,p) basis set[26] where the selection thresholds for the ground and excited states were 1.0×10^{-7} and 1.0×10^{-8}, respectively. By this calculation with polarization functions, we intended to show that the discrepancy of the calculation with the D95 basis can be improved by using better computational conditions. Considering probable errors arising from the lack of polarization functions, we can accept the qualitative discussion based on the calculation using the D95 basis because calculations with polarization functions are impossible for larger porphyrins.

The results of SAC-CI with polarization functions are also shown in Table III. The polarization functions did not affect the relative order of the B_{3u} and B_{2u} states; therefore, the qualitative assignment of absorption and MCD spectra can be accepted without polarization functions. The polarization functions particularly improved the excitation energies of the B_{2u} states. According to the calculation with polarization functions, the Q-bands observed at 2.00 and 2.25 eV are assigned to the $1B_{3u}$ and $1B_{2u}$ states, calculated at 1.93 and 2.34 eV, respectively. The shoulder of the B-band observed around 3.5 eV is the $2B_{3u}$ state calculated at 3.45 eV. The main peaks of the B-band observed at 3.60 and 3.91 eV correspond to the $2B_{2u}$ and $3B_{2u}$ states calculated at 3.71 and 4.09 eV, respectively. The deviation between the experiment and SAC-CI calculation was reduced to about 0.1 eV by using the polarization functions.

B. H_2Pc

Q-bands were observed at 1.78 and 1.87 eV in the absorption spectrum in solution.[16] They have, respectively, negative and positive MCD signals. The absorption energies in the vapor-phase experiment without *tert*-butyl groups[34] were 1.81 and 1.99 eV, respectively. If we assume that the

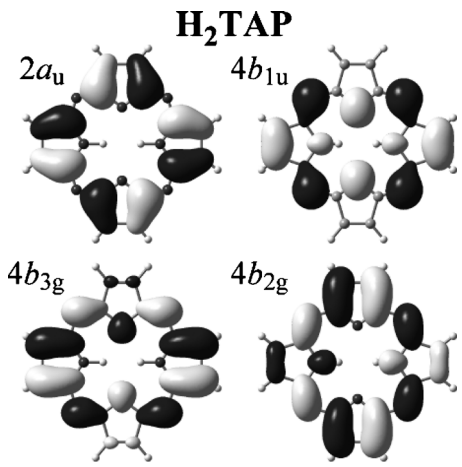

FIG. 3. Selected MOs of H_2TAP. The isosurfaces with contour value of 0.02 are shown.

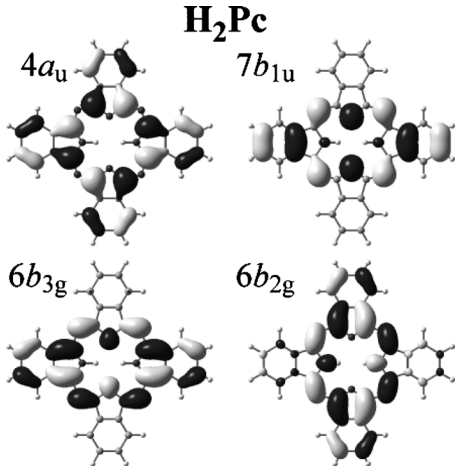

FIG. 4. Selected MOs of H_2Pc. The isosurfaces with contour value of 0.02 are shown.

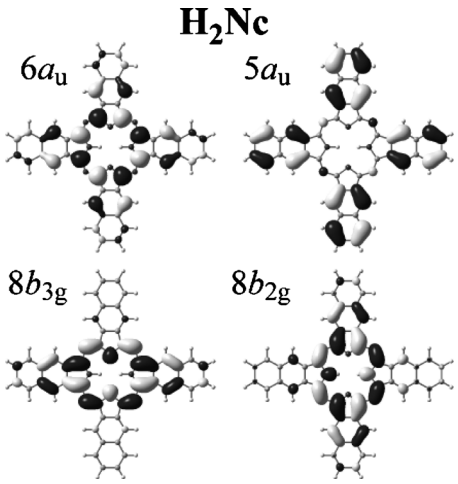

FIG. 5. Selected MOs of H_2Nc. The isosurfaces with contour value of 0.02 are shown.

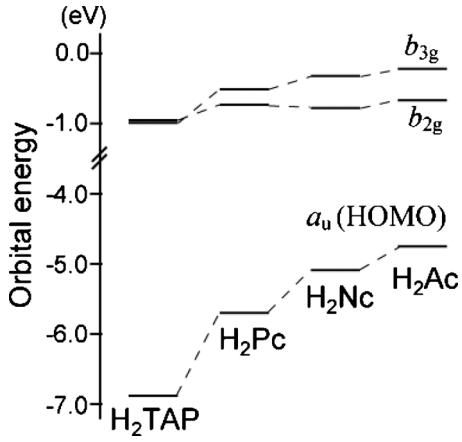

FIG. 7. Orbital energies of the HOMO (a_u), LUMO, and next-LUMO (b_{3g} and b_{2g}) in eV.

effect of *tert*-butyl groups is negligible, the solvent effect on the Q_y-band is considerable. The peak maximum of the B-band in solution was observed at 3.60 eV. Components of a broad B-band were observed at 3.5, 3.65, and 3.9 eV in the vapor-phase experiment. Pseudo-Faraday A-terms were observed at 3.44 and 3.78 eV by MCD spectroscopy. Other MCD signals were not identified between the 3.44 eV peak and the Q-bands.

The SAC-CI results are summarized in Table IV. Using the SAC-CI method, 21 states were calculated with excitation energies less than 4.5 eV. Among them eight states were optically allowed $\pi \rightarrow \pi^*$ excitations and two states were optically allowed $n \rightarrow \pi^*$ excitations. The $1B_{3u}$ and $1B_{2u}$ states are obviously Q-bands. The SAC-CI results well reproduced the excitation energies of the vapor-phase experiment. The next observed peak was the shoulder of the B-band of 3.5 eV observed in the vapor-phase experiment. This would correspond to the negative MCD peak at 3.44 eV. This absorption may be assigned to the $2B_{3u}$ state calculated at 3.47 eV. The other component of the pseudo-Faraday A-terms of the B-band was observed at 3.78 eV with a positive sign. This may correspond to the components of the B-band at 3.65 or 3.9 eV in the vapor-phase experiment. This absorption may be assigned to the $2B_{2u}$ state calculated at 3.94 eV. The next calculated $\pi \rightarrow \pi^*$ state was the $3B_{3u}$ state at 4.07 eV. This state may correspond to the peak observed at 3.9 eV in the vapor phase.

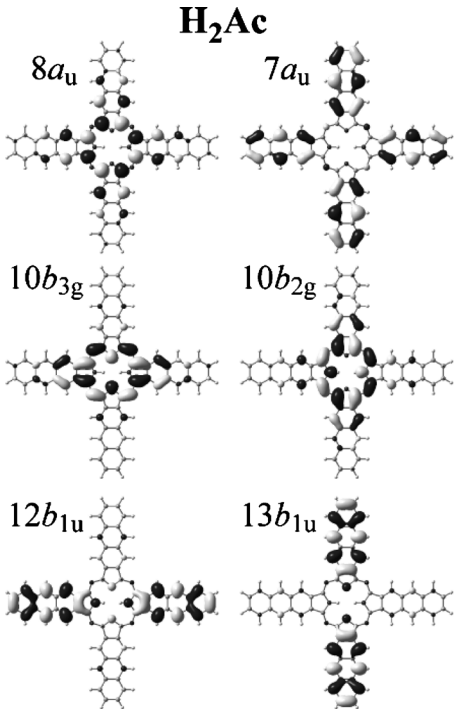

FIG. 6. Selected MOs of H_2Ac. The isosurfaces with contour value of 0.02 are shown.

If we adopt these assignments, the present SAC-CI calculation well reproduced the experimental excitation energies. The agreement between the calculation and experiment was better than that of H_2TAP. If we consider probable error of about 0.4 eV for this computational condition, it is possible to suggest another assignment as follows. The negative MCD term observed at 3.44 eV is broad and therefore we assume this peak is composed of two optically allowed states. Then the $2B_{3u}$ and $2B_{2u}$ states can be assigned to this peak. The remaining positive MCD term observed at 3.78 eV may be assigned to the $3B_{3u}$ state. To confirm the assignment in the B-band region of H_2Pc, we need to perform better computations.

C. H_2Nc

A single Q-band was observed at 1.58 eV in the absorption spectrum in solution. For this peak, the pseudo-Faraday A-terms of the energy at 1.56 and 1.59 eV were observed by MCD. The splitting of the Q-bands becomes smaller than the resolution of the absorption spectra in solution. A shoulder on the B-band beginning from 2.5 eV was observed in the absorption spectrum. In this region, a weak negative peak and a clear positive peak were observed at around 2.4 and 2.78 eV by MCD. Two peaks located at 3.42 and 3.79 eV were observed in the B-band region in the absorption spectrum. For the B-bands, a negative peak at 3.37 eV with a shoulder at around 3.18 eV and a positive peak at 3.89 eV were obtained by MCD.

TABLE III. SAC-CI results for H_2TAP compared with experimental results.

	SAC-CI[a]			SAC-CI[b]		Exp.		
State	Main configuration[c] ($\|d\|>0.3$)	EE[d]	Osc.[e]	EE	Osc.	Abs.[f]	MCD[g]	Abs.[h]
$1B_{3u}$	$0.74(2a_u\rightarrow 4b_{3g})+0.53(4b_{1u}\rightarrow 4b_{2g})$	2.06	0.113	1.93	0.197	2.00	2.00(−)	2.01
$1B_{2u}$	$0.81(2a_u\rightarrow 4b_{2g})-0.43(4b_{1u}\rightarrow 4b_{3g})$	2.59	0.208	2.34	0.240	2.25	2.25(+)	2.27
$1B_{2g}$	$0.90(14b_{1g}\rightarrow 4b_{3g})$	3.59	Forb.	3.67	Forb.			
$1B_{3g}$	$0.90(14b_{1g}\rightarrow 4b_{2g})$	3.59	Forb.	3.79	Forb.			
$2B_{3u}$	$0.67(3b_{1u}\rightarrow 4b_{2g})+0.43(4b_{1u}\rightarrow 4b_{2g})-0.40(2a_u\rightarrow 4b_{3g})$	3.63	0.440	3.45	0.373	~3.5	~3.5(−)	3.3
$1B_{1g}$	$0.89(3b_{3g}\rightarrow 4b_{2g})$	3.63	Forb.	3.48	Forb.			
$1A_u$	$0.85(17b_{2u}\rightarrow 4b_{2g})$	3.78	Forb.	3.91	Forb.			
$1B_{1u}$	$0.90(17b_{2u}\rightarrow 4b_{3g})-0.35(17b_{3u}\rightarrow 4b_{2g})$	3.83	0.013	3.90	0.025			
$2B_{2u}$	$0.66(4b_{1u}\rightarrow 4b_{3g})+0.54(3b_{1u}\rightarrow 4b_{3g})$	3.94	0.566	3.71	0.434	3.71	3.60(−)	3.72
$2B_{1u}$	$0.81(17b_{3u}\rightarrow 4b_{2g})-0.39(17b_{2u}\rightarrow 4b_{3g})$	4.07	0.000	4.25	0.001			
$2B_{2g}$	$0.90(20a_g\rightarrow 4b_{2g})$	4.08	Forb.	4.11	Forb.			
$2A_u$	$0.89(17b_{3u}\rightarrow 4b_{3g})$	4.09	Forb.	4.19	Forb.			
$1A_g$	$0.79(3b_{3g}\rightarrow 4b_{3g})+0.36(2a_u\rightarrow 3a_u)$	4.11	Forb.	4.15	Forb.			
$3B_{2u}$	$0.72(2b_{1u}\rightarrow 4b_{3g})+0.46(3b_{1u}\rightarrow 4b_{3g})$	4.29	0.403	4.09	0.398		3.91(+)	
$2B_{3g}$	$0.91(20a_g\rightarrow 4b_{3g})$	4.35	Forb.	4.31	Forb.			
$3B_{3u}$	$0.55(3b_{1u}\rightarrow 4b_{2g})-0.47(4b_{1u}\rightarrow 4b_{2g})+0.44(2b_{1u}\rightarrow 4b_{2g})$	4.35	0.984	4.29	1.022			
$2B_{1g}$	$0.86(3b_{2g}\rightarrow 4b_{3g})$	4.41	Forb.	4.23	Forb.			
$2A_g$	$0.73(2a_u\rightarrow 3a_u)-0.42(3b_{3g}\rightarrow 4b_{3g})$	4.45	Forb.	4.31	Forb.			

[a]SAC-CI calculation with the D95 basis.
[b]SAC-CI calculation with the D95(d,p) basis and tighter threshold, see text.
[c]Main configurations of the SAC-CI wave function whose absolute value of the coefficient is larger than 0.3 are shown.
[d]Excitation energy in eV.
[e]Oscillator strength.
[f]UV-vis absorption spectrum in pyridine for H_2TAP with *tert*-butyl group from Ref. 16.
[g]MCD spectrum in pyridine for H_2TAP with *tert*-butyl group from Ref. 16; the signs of the MCD signal are given in parentheses.
[h]UV-vis absorption spectrum in chlorobenzene from Ref. 33.

The SAC-CI results are summarized in Table V. Using the SAC-CI method, 27 states were calculated with excitation energies less than 4.5 eV. Among them, ten states were optically allowed $\pi\rightarrow\pi^*$ excitations and two states were optically allowed $n\rightarrow\pi^*$ excitations. The $1B_{3u}$ and $1B_{2u}$ states are obviously Q-bands. The SAC-CI results reasonably reproduced the experimental excitation energies, although the energy of the $1B_{2u}$ state was slightly overestimated. The splitting of the two Q-bands was thus slightly overestimated by the SAC-CI calculation.

For the B-band region, we simply assign optically allowed $\pi\rightarrow\pi^*$ states to MCD peaks according to the calculated energy sequence. The negative and positive peaks for the B-band shoulder observed at 2.4 and 2.78 eV were assigned to the $2B_{2u}$ and $2B_{3u}$ states, respectively, even though the deviations of the calculated excitation energies are large. The shoulder of the negative peak observed at 3.18 eV may be assigned to the $3B_{2u}$ or $3B_{3u}$ states calculated at 3.40 and 3.53 eV. The next negative peak observed at 3.37 eV may be the $4B_{3u}$ state calculated at 3.63 eV. The positive peak observed at 3.89 eV may be assigned to the $4B_{2u}$ and $5B_{3u}$ states calculated at 3.88 and 3.90 eV. In this region, errors of the calculation seem to be reasonable; they are about 0.3 eV or less. The reason is unclear for the relatively large deviations of the $2B_{2u}$ and $2B_{3u}$ states from experiment for this compound. To verify these assignments we need to calculate MCD rotational strengths with sufficient accuracy.

D. H_2Ac

A single absorption at 1.44 eV was observed for the Q-bands of H_2Ac, where the pseudo-Faraday A-terms of 1.42 and 1.45 eV were observed by MCD. Two small peaks at 2.19 and 2.52 eV were observed before the strong B-band at 3.52 eV and its shoulder at 3.06 eV. For the region between the Q- and B-bands, two positive signals at 2.19 and 2.42 eV and a negative signal at about 2.76 eV were observed by MCD. A strong negative MCD signal was observed at 3.03 eV, which would correspond to the shoulder in the absorption spectrum of 3.06 eV. Notably complex components were observed by MCD for the broad B-band whose absorption maximum was 3.52 eV. Positive signals were observed at 3.15 and 3.29 eV. Then negative and positive signals were observed at 3.44 and 3.59 eV, respectively.

The SAC-CI results are summarized in Table VI. Using the SAC-CI method, 38 states were calculated with excitation energies less than 4.5 eV. Among them, 17 states were optically allowed $\pi\rightarrow\pi^*$ excitations and two states were optically allowed $n\rightarrow\pi^*$ excitations. The calculated excitation energies of the $1B_{3u}$ and $1B_{2u}$ states that correspond to Q-bands were 1.26 and 1.30 eV, respectively. The SAC-CI calculation underestimated the excitation energies by about 0.15 eV. The calculated splitting of these bands agrees well with the experimental findings.

For peaks other than Q-bands, we simply assign calculated states according to the energy order. For the energy region 2–3 eV, the $2B_{2u}$, $3B_{2u}$, and $3B_{3u}$ states are assigned to the MCD peaks of 2.19, 2.42, and 2.76 eV, respectively.

TABLE IV. SAC-CI results for H_2Pc compared with experimental results.

	SAC-CI			Exp.		
State	Main configuration[a] ($\|d\|>0.3$)	EE[b]	Osc[c]	Abs.[d]	MCD[e]	Abs.[f]
$1B_{3u}$	$0.82(4a_u\rightarrow 6b_{3g})+0.39(7b_{1u}\rightarrow 6b_{2g})$	1.83	0.387	1.78	1.78(−)	1.81
$1B_{2u}$	$0.88(4a_u\rightarrow 6b_{2g})$	2.11	0.707	1.87	1.87(+)	1.99
$2B_{3u}$	$0.60(6b_{1u}\rightarrow 6b_{2g})-0.58(7b_{1u}\rightarrow 6b_{2g})$	3.47	0.655	3.60	3.44(−)	3.5
$1B_{1g}$	$0.88(5b_{3g}\rightarrow 6b_{2g})$	3.51	Forb.			
$1B_{3g}$	$0.90(24b_{1g}\rightarrow 6b_{2g})$	3.52	Forb.			
$1B_{2g}$	$0.90(24b_{1g}\rightarrow 6b_{3g})$	3.67	Forb.			
$1A_u$	$0.90(28b_{2u}\rightarrow 6b_{2g})$	3.76	Forb.			
$1A_g$	$0.83(4a_u\rightarrow 5a_u)$	3.80	Forb.			
$2B_{2u}$	$0.77(7b_{1u}\rightarrow 6b_{3g})$	3.94	1.164		3.78(+)	3.65
$1B_{1u}$	$0.86(28b_{2u}\rightarrow 6b_{3g})$	3.96	0.010			
$2B_{1u}$	$0.87(28b_{3u}\rightarrow 6b_{2g})$	4.03	0.001			
$3B_{3u}$	$0.65(6b_{1u}\rightarrow 6b_{2g})+0.48(7b_{1u}\rightarrow 6b_{2g})$	4.07	1.845			3.9
$2A_g$	$0.75(5b_{2g}\rightarrow 6b_{2g})+0.35(5b_{3g}\rightarrow 6b_{3g})$	4.08	Forb.			
$2B_{2g}$	$0.90(32a_g\rightarrow 6b_{2g})$	4.08	Forb.			
$2A_u$	$0.89(28b_{3u}\rightarrow 6b_{3g})$	4.21	Forb.			
$3A_g$	$0.63(5b_{3g}\rightarrow 6b_{3g})+0.40(5b_{2g}\rightarrow 6b_{2g})-0.31(5b_{2g}\rightarrow 6b_{2g})$	4.24	Forb.			
$2B_{1g}$	$0.88(4a_u\rightarrow 8b_{1u})$	4.29	Forb.			
$3B_{2u}$	$0.83(5b_{1u}\rightarrow 6b_{3g})$	4.31	0.062			
$4B_{2u}$	$0.77(3a_u\rightarrow 6b_{2g})$	4.43	0.037			
$2B_{3g}$	$0.89(32a_g\rightarrow 6b_{3g})$	4.43	Forb.			
$4B_{3u}$	$0.54(5b_{1u}\rightarrow 6b_{2g})+0.44(3a_u\rightarrow 6b_{3g})$	4.47	0.057			

[a]Main configurations of the SAC-CI wave function whose absolute value of the coefficient is larger than 0.3 are shown.
[b]Excitation energy in eV.
[c]Oscillator strength.
[d]UV-vis absorption spectrum in pyridine for H_2Pc with *tert*-butyl group from Ref. 16.
[e]MCD spectrum in pyridine for H_2Pc with *tert*-butyl group from Ref. 16; the signs of the MCD signal are given in parentheses.
[f]UV-vis absorption spectrum in the vapor phase from Ref. 34.

The deviations between calculated and observed excitation energies are about 0.3–0.4 eV. They are not small, but the error is acceptable within the present computational conditions. For the B-band region, the $4B_{3u}$, $4B_{2u}$, $5B_{3u}$, $6B_{3u}$, and $5B_{2u}$ states may be assigned to the MCD peaks of 3.03, 3.15, 3.29, 3.44, and 3.59 eV, respectively. Under the assumption of this assignment, the deviations between calculated and observed excitation energies were about 0.25–0.4 eV.

V. RELATIONS BETWEEN MOLECULES

A. Overall trends of excitations

The number of valence π-orbitals increases in accordance with the extension of the molecular size. Therefore, the larger molecules can have a larger number of electron transitions in the low-energy region than that of small molecules. This makes the spectra complicated. Here, we will discuss the correlations of excited states between the TAP derivatives based on the similarity of MO characters. This analysis will be helpful in understanding series properties of electron excitations for such π-extended porphyrins.

The four-orbital model gives a basic understanding of electronic excitations of porphyrins; the model states that the Q- and B-bands are the electron transitions between the HOMO/next-HOMO and the LUMO/next-LUMO.[4] This explanation is significant as the principal approximation. For H_2TAP, the Q-bands are the $1B_{2u}$ and $1B_{3u}$ states and the B-bands are the $2B_{3u}$ and $2B_{2u}$ states. Figure 9 shows the correspondence of these four states to those in other compounds. For these four compounds, the Q-bands are the $1B_{2u}$ and $1B_{3u}$ states, in which the orbital characters related to electron transition are similar between the series of compounds. The excitation energies of the Q-bands shift to low energy with the extension of molecular size and the energy difference between the $1B_{2u}$ and $1B_{3u}$ states becomes small.[2,15,16] Such behavior of Q-bands will be discussed in the next subsection.

For H_2Pc and H_2Nc, $2B_{3u}$ is the state that corresponds to the $2B_{3u}$ state of H_2TAP in terms of orbital character. The analogous states in H_2Ac are the $4B_{3u}$ and $6B_{3u}$ states; they have complex main configurations, as shown in Table VI. Excitations from π-orbitals other than the next-HOMO, namely, $10b_{1u}$ and $9b_{1u}$ orbitals, significantly contributed to these states. The states that correspond to the $2B_{2u}$ state of H_2TAP in terms of orbital character are, respectively, the $2B_{2u}$ and $4B_{2u}$ for H_2Pc and H_2Nc. The analogous states of H_2Ac are the $5B_{2u}$ and $6B_{2u}$ that also involved contributions from π-orbitals other than the next-HOMO. As shown in Table VI, these states also had complex main configurations. The correspondence of the states between H_2TAP and H_2Ac in the B-band region is not so good because $\pi\rightarrow\pi^*$ excitations other than the four orbitals mix to them. In comparison with the Q-bands, the energy shifts with the extension of molecular size are small for the B-bands.

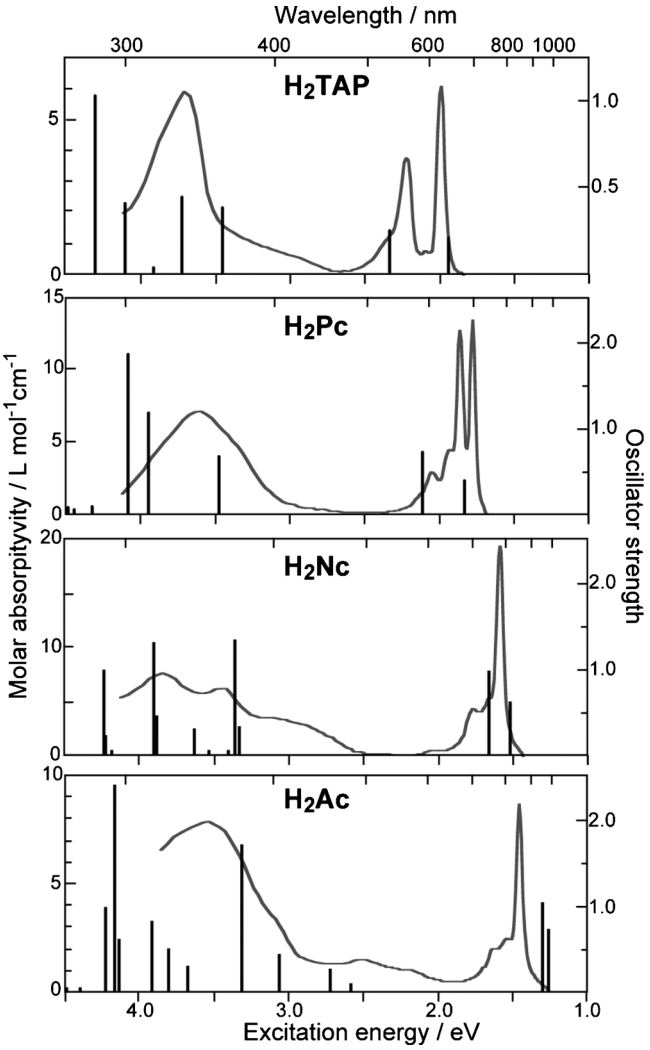

FIG. 8. Observed absorption spectra (Ref. 16) and the SAC-CI results shown as vertical lines. The horizontal axis of the spectra in Ref. 16 was converted into an energy scale from a wavelength scale. For H_2TAP, the result with D95(d,p) basis is shown.

In H_2Ac, there are calculated states that do not correspond to low-lying excited states of H_2TAP because the number of valence π-electrons is different. For H_2Ac, the $2B_{2u}$ and $2B_{3u}$ are the optically allowed states that have low excitation energies next to the Q-bands. They are the electron transition from HOMO to the unoccupied orbitals over the next-LUMO. The states with similar character of electron transition are the $3B_{2u}$ and $3B_{3u}$ for H_2Nc. The calculated excitation energies are 3.40 and 3.53 eV; they are about 0.8 eV higher than those of H_2Ac. The corresponding states were not obtained by the SAC-CI calculations within the present energy range for H_2Pc and H_2TAP.

The next optically allowed transitions for H_2Ac are the $3B_{2u}$ and $3B_{3u}$ states. They are the transitions from the $7a_u$ orbital to the LUMO and next-LUMO. These states relate to the Q-bands but their orbital characters are different. The isosurfaces of the $7a_u$ and $8a_u$ orbitals are shown in Fig. 6. The HOMO $8a_u$ orbital has a large electron distribution around porphin, while the $7a_u$ orbital has a large electron distribution in the anthracene groups. The LUMO and next-LUMO have a distribution mainly around porphin. Consequently, the $3B_{2u}$ and $3B_{3u}$ states, transitions from the $7a_u$ to the LUMO/next-LUMO, have the character of intramolecular charge transfer from the peripheral anthracene groups to the central porphin part. The corresponding states for H_2Nc are the $2B_{2u}$ and $4B_{3u}$ states and those for H_2Pc are the $4B_{2u}$ and $4B_{3u}$ states. The excitation energies for these states shift to higher energy in accordance with the reduction in molecular size.

In the UV-vis spectrum of H_2Ac, absorptions are observed in the region between the Q- and B-bands around 2–3 eV. The $2B_{2u}$, $2B_{3u}$, $3B_{2u}$, and $3B_{3u}$ states, discussed above, correspond to these absorptions by the SAC-CI calculations. In the absorption spectrum of H_2Nc, the corresponding absorptions shift to the higher energy region covered by the B-bands. Such relations are shown in Fig. 9. The energies of these states strongly depend on the molecular size.

The lowest optically forbidden states are the $1B_{2g}$ and $1B_{3g}$ for H_2TAP; they are $n \rightarrow \pi^*$ transitions. For the other molecules, the $1B_{2g}$ and $1B_{3g}$ states have the same character as those of H_2TAP. The excitation energies of $1B_{2g}$ states are 3.5–3.6 eV for these molecules; they are approximately constant among these molecules. The excitation energies of the $1B_{3g}$ states shift to lower energy in accordance with the extension of molecular size; however, the shift is small.

For H_2Ac, the $1B_{1g}$ and $2B_{1g}$ states are calculated at 2.31 and 2.63 eV. They are the excitation from the $8a_u$ (HOMO) to the $12b_{1u}$ and $13b_{1u}$ orbitals, respectively. The orbital distributions of the $12b_{1u}$ and $13b_{1u}$ are quite different. As shown in Fig. 6, the $12b_{1u}$ orbital extends along the x-direction, while the $13b_{1u}$ orbital extends along the y-direction. The corresponding states for H_2Nc are the $1B_{1g}$ and $3B_{1g}$ states, respectively, whose excitation energies are 3.04 and 3.50 eV. The excitation energies rose in H_2Nc; additionally, the energy difference between these two states increased. For H_2Pc, the x-direction $2B_{1g}$ state was calculated at 4.29 eV; however, the corresponding state for the y-direction did not exist in the energy region of the present calculations. Even though they are optically forbidden, they are quite interesting states because of their significantly different electronic distribution in the same irreducible representation. We suppose a possibility of these states working as a molecular switch that controls an electric current. A single molecular switch of H_2Nc has already been reported.[35]

B. Q-bands

The characteristics of absorption of the Q-bands and MCD spectra have been pointed out in Ref. 16; here, we discuss the Q-bands calculated with the SAC-CI method. The observed absorption coefficients of the Q-bands increase in the order H_2TAP, H_2Pc, and H_2Nc. The coefficients of H_2Ac were slightly smaller than those of H_2Nc. The oscillator strengths of the Q-bands calculated using SAC-CI increase in the same manner as the experimental findings, although the calculated oscillator strengths of H_2Ac are slightly larger than those of H_2Nc.

The Q-band shifts to lower energy in accordance with extension of the systems, but the energy shifts decrease with

TABLE V. SAC-CI results for H_2Nc compared with experimental results.

	SAC-CI			Exp.	
State	Main configuration[a] ($\|d\|>0.3$)	EE[b]	Osc[c]	Abs.[d]	MCD[e]
$1B_{3u}$	$0.86(6a_u\rightarrow 8b_{3g})$	1.52	0.616	1.58	1.56(−)
$1B_{2u}$	$0.90(6a_u\rightarrow 8b_{2g})$	1.66	0.974		1.59(+)
$1B_{1g}$	$0.88(6a_u\rightarrow 10b_{1u})$	3.04	Forb.		
$1A_g$	$0.79(7b_{2g}\rightarrow 8b_{2g})$	3.28	Forb.		
$2B_{2u}$	$0.83(5a_u\rightarrow 8b_{2g})$	3.33	0.325	<2.5	~2.4(−)
$2B_{3u}$	$0.79(9b_{1u}\rightarrow 8b_{2g})$	3.36	1.331		2.78(+)
$1B_{3g}$	$0.90(34b_{1g}\rightarrow 8b_{2g})$	3.39	Forb.		
$3B_{2u}$	$0.90(6a_u\rightarrow 9b_{2g})$	3.40	0.004		3.18(−) (sh)
$2A_g$	$0.75(6a_u\rightarrow 7a_u)-0.31(7b_{2g}\rightarrow 8b_{2g})$	3.40	Forb.		
$2B_{1g}$	$0.60(7b_{3g}\rightarrow 8b_{2g})-0.49(6a_u\rightarrow 11b_{1u})-0.35(6b_{3g}\rightarrow 8b_{2g})$	3.45	Forb.		
$3B_{1g}$	$0.83(6a_u\rightarrow 11b_{1u})+0.32(7b_{3g}\rightarrow 8b_{2g})$	3.50	Forb.		
$3B_{3u}$	$0.84(6a_u\rightarrow 9b_{3g})$	3.53	0.032		
$4B_{3u}$	$0.76(5a_u\rightarrow 8b_{3g})$	3.63	0.241	3.42	3.37(−)
$1B_{2g}$	$0.90(34b_{1g}\rightarrow 8b_{3g})$	3.63	Forb.		
$1A_u$	$0.90(39b_{2u}\rightarrow 8b_{2g})$	3.66	Forb.		
$3A_g$	$0.77(7b_{3g}\rightarrow 8b_{3g})-0.36(6a_u\rightarrow 7a_u)$	3.68	Forb.		
$4B_{1g}$	$0.67(7b_{2g}\rightarrow 8b_{3g})+0.50(6b_{3g}\rightarrow 8b_{2g})$	3.76	Forb.		
$5B_{1g}$	$0.58(7b_{2g}\rightarrow 8b_{3g})-0.49(6b_{3g}\rightarrow 8b_{2g})-0.48(7b_{3g}\rightarrow 8b_{2g})$	3.88	Forb.		
$4B_{2u}$	$0.65(9b_{1u}\rightarrow 8b_{3g})+0.39(7b_{1u}\rightarrow 8b_{3g})-0.36(4a_u\rightarrow 8b_{2g})$	3.88	0.425		
$5B_{3u}$	$0.82(8b_{1u}\rightarrow 8b_{2g})$	3.90	1.302	3.79	3.89(+)
$1B_{1u}$	$0.71(39b_{2u}\rightarrow 8b_{3g})-0.55(39b_{3u}\rightarrow 8b_{2g})$	3.91	0.002		
$2B_{1u}$	$0.70(39b_{3u}\rightarrow 8b_{2g})+0.53(39b_{2u}\rightarrow 8b_{3g})$	3.97	0.008		
$2B_{2g}$	$0.89(44a_g\rightarrow 8b_{2g})$	4.00	Forb.		
$2A_u$	$0.88(39b_{3u}\rightarrow 8b_{3g})$	4.16	Forb.		
$5B_{2u}$	$0.55(4a_u\rightarrow 8b_{2g})+0.54(9b_{1u}\rightarrow 8b_{3g})-0.36(7b_{1u}\rightarrow 8b_{3g})$	4.18	0.025		
$6B_{3u}$	$0.45(7b_{1u}\rightarrow 8b_{2g})+0.42(4a_u\rightarrow 8b_{3g})+0.39(5a_u\rightarrow 8b_{3g})$	4.22	0.221		
$6B_{2u}$	$0.45(8b_{1u}\rightarrow 8b_{3g})-0.39(7b_{1u}\rightarrow 8b_{3g})$	4.23	1.670		
$4A_g$	$0.76(6b_{3g}\rightarrow 8b_{3g})$	4.36	Forb.		
$2B_{3g}$	$0.88(44a_g\rightarrow 8b_{3g})$	4.41	Forb.		
$7B_{2u}$	$0.55(8b_{1u}\rightarrow 8b_{3g})+0.52(8b_{1u}\rightarrow 8b_{3g})+0.44(4a_u\rightarrow 8b_{2g})$	4.45	Forb.		

[a]Main configurations of the SAC-CI wave function whose absolute value of the coefficient is larger than 0.3 are shown.
[b]Excitation energy in eV.
[c]Oscillator strength.
[d]UV-vis absorption spectrum in pyridine for H_2Nc with *tert*-butyl group from Ref. 16.
[e]MCD spectrum in pyridine for H_2Nc with *tert*-butyl group from Ref. 16; the signs of the MCD signal are given in parentheses.

increasing molecular size. If we take the center of two Q-bands, the energy shift between H_2TAP and H_2Pc, that between H_2Pc and H_2Nc, and that between H_2Nc and H_2Ac are 0.30, 0.25, and 0.14 eV, respectively, from the absorption spectra in solution. This characteristic of redshifts can be simply explained by the orbital energy levels of the HOMO, LUMO, and next-LUMO; they are illustrated in Fig. 7. By the four-orbital model, Q-bands are described by the transition between HOMO and LUMO and that between HOMO and next-LUMO. The orbital energies of the HOMO increase in accordance with the extension of the systems, but the increment is suppressed in larger systems. This trend agrees well with the energy shifts of the Q-bands and is clearly understood by Fig. 7; as has already been pointed out.[16,18]

The SAC-CI calculations reproduced the lower energy shift; however, the calculated shift values did not monotonically decrease with increasing molecular size. From the SAC-CI calculations, the energy shifts between H_2TAP and H_2Pc, between H_2Pc and H_2Nc, and between H_2Nc and H_2Ac are 0.36, 0.38, and 0.31 eV, respectively. The shift between H_2Pc and H_2Nc is the largest, which contradicts the experimental findings. We assume this discrepancy is attributed to the perturbation-selection used in the SAC-CI calculations. In larger systems, contributions of some important double excitations may be divided into small contributions and be dispersed over the molecule because of the extension of MOs. Therefore, one should use tighter thresholds for larger molecules to collect such diluted contributions; however, the current computer resources limited our calculations.

The splitting of the Q-bands decreases in accordance with the extension of the systems; the split Q-band did not appear in the absorption spectra of H_2Nc and H_2Ac. This trend was reproduced by the SAC-CI calculations. Moreover, we found that this characteristic was not explained by a simple orbital model because the energy differences between the LUMO and next-LUMO are not proportional to the splitting of the Q-bands. This point will be discussed in the next section.

TABLE VI. SAC-CI results for H_2Ac compared with experimental results.

	SAC-CI			Exp.	
State	Main configuration[a] ($\|d\|>0.3$)	EE[b]	Osc.[c]	Abs.[d]	MCD[e]
$1B_{3u}$	$0.87(8a_u \rightarrow 10b_{3g})$	1.26	0.733	1.44	1.42(−)
$1B_{2u}$	$0.91(8a_u \rightarrow 10b_{2g})$	1.30	1.037		1.45(+)
$1B_{1g}$	$0.89(8a_u \rightarrow 12b_{1u})$	2.31	Forb.		
$2B_{2u}$	$0.89(8a_u \rightarrow 11b_{2g})$	2.58	0.071	2.19	2.19(+)
$2B_{1g}$	$0.89(8a_u \rightarrow 13b_{1u})$	2.63	Forb.		
$2B_{3u}$	$0.88(8a_u \rightarrow 11b_{3g})$	2.67	0.002		
$3B_{2u}$	$0.87(7a_u \rightarrow 10b_{2g})$	2.72	0.267	2.52	2.42(+)
$1A_g$	$0.82(9b_{2g} \rightarrow 10b_{2g})$	2.82	Forb.		
$3B_{1g}$	$0.86(9b_{3g} \rightarrow 10b_{2g})$	2.91	Forb.		
$3B_{3u}$	$0.84(7a_u \rightarrow 10b_{3g})$	3.06	0.442		2.76(−)
$2A_g$	$0.63(9b_{3g} \rightarrow 10b_{3g}) + 0.47(8a_u \rightarrow 9a_u)$	3.07	Forb.		
$1B_{3g}$	$0.89(44b_{1g} \rightarrow 10b_{2g})$	3.23	Forb.		
$4B_{1g}$	$0.87(9b_{2g} \rightarrow 10b_{3g})$	3.26	Forb.		
$3A_g$	$0.69(8a_u \rightarrow 9a_u) - 0.50(9b_{3g} \rightarrow 10b_{3g})$ $0.60(11b_{1u} \rightarrow 10b_{2g}) + 0.39(9b_{1u} \rightarrow 10b_{2g}) - 0.36(10b_{1u}$	3.31	Forb.		
$4B_{3u}$	$\rightarrow 10b_{2g})$	3.31	1.711	3.06	3.03(−)
$4B_{2u}$	$0.78(6a_u \rightarrow 10b_{2g})$	3.42	0.033	(sh)	3.15(+)
$1A_u$	$0.89(50b_{2u} \rightarrow 10b_{2g})$	3.47	Forb.		
$1B_{2g}$	$0.89(44b_{1g} \rightarrow 10b_{3g})$	3.53	Forb.		
$5B_{3u}$	$0.53(6a_u \rightarrow 10b_{3g}) + 0.32(10b_{1u} \rightarrow 10b_{2g})$	3.67	0.302	3.52	3.29(+)
$6B_{3u}$	$0.57(11b_{1u} \rightarrow 10b_{2g}) + 0.54(10b_{1u} \rightarrow 10b_{2g})$	3.80	0.490		3.44(−)
$1B_{1u}$	$0.67(50b_{2u} \rightarrow 10b_{3g}) - 0.59(50b_{3u} \rightarrow 10b_{2g})$	3.85	0.001		
$5B_{1g}$	$0.70(8b_{3g} \rightarrow 10b_{2g})$	3.87	Forb.		
$2B_{2g}$	$0.88(56a_g \rightarrow 10b_{2g})$	3.87	Forb.		
$5B_{2u}$	$0.38(10b_{1u} \rightarrow 10b_{3g}) - 0.36(8b_{3g} \rightarrow 13b_{1u}) - 0.36(9b_{1u} \rightarrow 10b_{3g}) - 0.33(11b_{1u} \rightarrow 11b_{3g})$	3.91	0.820		3.59(+)
$2B_{1u}$	$0.65(50b_{3u} \rightarrow 10b_{2g}) + 0.59(50b_{3u} \rightarrow 10b_{2g})$	3.94	0.008		
$4A_g$	$0.45(8b_{3g} \rightarrow 10b_{3g}) - 0.36(8b_{3g} \rightarrow 11b_{3g}) - 0.35(11b_{1u} \rightarrow 13b_{1u}) - 0.34(8a_u \rightarrow 10a_u)$	3.95	Forb.		
$6B_{2u}$	$0.52(11b_{1u} \rightarrow 10b_{3g}) - 0.33(10b_{1u} \rightarrow 10b_{3g}) - 0.32(9b_{3g} \rightarrow 12b_{1u})$	3.99	0.001		
$5A_g$	$0.54(8b_{2g} \rightarrow 10b_{2g}) + 0.34(10b_{1u} \rightarrow 12b_{1u})$	4.07	Forb.		
$2A_u$	$0.86(50b_{3u} \rightarrow 10b_{3g})$	4.09	Forb.		
$6B_{1g}$	$0.56(9b_{3g} \rightarrow 11b_{2g}) + 0.36(6a_u \rightarrow 12b_{1u}) - 0.35(7a_u \rightarrow 13b_{1u}) - 0.33(9b_{2g} \rightarrow 12b_{1u})$	4.09	Forb.		
$7B_{3u}$	$0.52(9b_{2g} \rightarrow 13b_{1u}) + 0.42(7a_u \rightarrow 11b_{3g})$	4.13	0.609		
$7B_{2u}$	$0.43(9b_{3g} \rightarrow 12b_{1u}) + 0.38(9b_{1u} \rightarrow 10b_{3g}) - 0.35(7a_u \rightarrow 11b_{2g})$	4.16	2.402		
$8B_{3u}$	$0.53(8a_u \rightarrow 12b_{3g}) + 0.50(6a_u \rightarrow 10b_{3g})$	4.22	0.978		
$2B_{3g}$	$0.87(56a_g \rightarrow 10b_{3g})$	4.33	Forb.		
$3A_u$	$0.81(49b_{2u} \rightarrow 10b_{2g}) - 0.32(48b_{2u} \rightarrow 10b_{2g})$ $0.52(9b_{1u} \rightarrow 10b_{3g}) - 0.46(11b_{1u} \rightarrow 10b_{3g}) + 0.32(10b_{1u}$	4.39	Forb.		
$8B_{2u}$	$\rightarrow 10b_{3g})$	4.39	0.046		
$6A_g$	$0.69(8b_{3g} \rightarrow 10b_{3g}) + 0.31(8b_{3g} \rightarrow 11b_{3g})$	4.42	Forb.		
$9B_{3u}$	$0.63(8a_u \rightarrow 12b_{2g}) + 0.63(8a_u \rightarrow 13b_{2g})$	4.48	0.036		

[a]Main configurations of the SAC-CI wave function whose absolute value of the coefficient is larger than 0.3 are shown.
[b]Excitation energy in eV.
[c]Oscillator strength.
[d]UV-vis absorption spectrum in pyridine for H_2Ac with *tert*-butyl group from Ref. 16.
[e]MCD spectrum in pyridine for H_2Ac with *tert*-butyl group from Ref. 16; the signs of the MCD signal are given in parentheses.

VI. Q BAND SPLITTING: COMPARISON WITH OTHER METHODS

The redshifts of the Q-bands can be explained by the orbital energy level of the HOMO, while the splitting of the Q-bands cannot be explained by the orbital energy levels of the LUMO and next-LUMO. To study this point further we performed calculations of excitation energies of the Q-bands using CIS, CIS(D), and TDDFT methods. The results are shown in Table VII with the experimental excitation energies obtained by MCD.

By the CIS calculations, in which electron correlation is not considered, the $1B_{3u}$ state had a lower energy than $1B_{2u}$

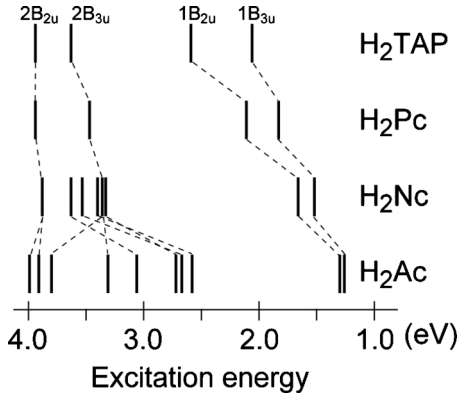

FIG. 9. Correlation diagram of selected optically allowed $\pi \rightarrow \pi^*$ states in H_2TAP, H_2Pc, H_2Nc, and H_2Ac.

for H_2TAP. For H_2Pc, H_2Nc, and H_2Ac, the energy order between B_{2u} and B_{3u} was inverted. Comparing with experiment, the CIS calculations overestimated the excitation energies for about 0.5 eV. Moreover, the energy difference between $1B_{2u}$ and $1B_{3u}$ states was the smallest in H_2Pc and largest in H_2Ac. This behavior does not agree with the trend of the experimental observations.

The lowest order of electron correlation can be considered by the CIS(D) method for electronic excitations, where the second-order many-body perturbation is used for the ground and the CIS excited sates. By the CIS(D) calculations, the $1B_{3u}$ states had a lower energy than the $1B_{2u}$ states for all these TAP compounds. This indicates that the electron correlations in the B_{3u} and B_{2u} states are significantly different. For all of these molecules, the differences between CIS and CIS(D) were about 0.2 and 0.5 eV in the B_{3u} and B_{2u} states, respectively. The calculated excitation energies by CIS(D) were higher than those of the CIS calculations; therefore, the agreement with experiment was not improved by using the CIS(D) method. This discrepancy may be attributed to the unbalanced treatment of electron correlations in the ground and excited states. The observed trend that the splitting of Q-bands decreases with the extension of the molecules was reproduced by the CIS(D) calculation. The splitting values of the Q-bands are similar to those obtained by the SAC-CI calculations; therefore, the relative energies for the B_{2u} and B_{3u} states can be well described by the CIS(D) method.

These results clearly show that the dynamic correlation that is considered by second-order many-body perturbation theory is essential to describe the relative energies of the B_{2u} and B_{3u} states and to explain the splitting values of the Q-bands of free-base porphyrins. The differences between the B_{2u} and B_{3u} states in the free-base molecules originate from the inner hydrogens; therefore, proper descriptions of both protonated nitrogens and nitrogen lone pairs are necessary to explain these differences. The interaction between the protonated nitrogens may be considered as an interaction of the polar N–H bonds. Then, the electrostatic component may be dominant. The interaction between lone pairs would be significantly affected by the electron correlation because there are important electron-electron interactions in a relatively small region. Consequently, the competition of these effects would decrease the splitting of the Q-bands. To understand the origin of such properties we require a detailed analysis of the wave function, including electron correlation effects. Such an analysis beyond the MO level may be associated with natural orbitals of the SAC-CI wave functions; this will appear in our future work.

Nowadays TDDFT calculations are widely applied to study of excited electronic states of large molecules. Thus we performed TDDFT calculations for the excitation energies of Q-bands for these molecules. The results are shown in Table VII. The excitation energies calculated by B3LYP were lower than those of the CIS results. The differences from the CIS results became larger in the larger molecules; the differences were about 0.1 eV for H_2TAP and were about 0.3 eV for H_2Ac. The differences from the CIS were about 0.05 eV larger in the B_{3u} than in the B_{2u} state. Comparing with experiment, the B3LYP calculation overestimated the excitation energies of the Q-bands by about 0.4 eV and by about 0.2 eV in H_2TAP and H_2Ac, respectively. For the splitting of the Q-bands, the trend of the B3LYP results was similar to the trend of the CIS calculation; the Q-bands were hardly split in H_2Pc and the split width was the largest in H_2Ac. This trend is inconsistent with the experimental findings. We

TABLE VII. Comparison of the excitation energies of the Q-bands states by several methods.

		CIS		CIS(D)		SAC-CI		B3LYP		BLYP		LC-BLYP		Exp	
		EE[a]	ΔE [b]	EE	ΔE	EE	ΔE	EE	ΔE	EE	ΔE	EE	ΔE	EE	ΔE
H_2TAP	$1B_{3u}$	2.54	0.13	2.67	0.45	2.06	0.53	2.44	0.15	2.32	0.14	2.13	0.29	2.01	0.26
	$1B_{2u}$	2.67		3.12		2.59		2.59		2.46		2.42		2.27	
H_2Pc	$1B_{3u}$	2.27	−0.05	2.50	0.23	1.83	0.28	2.12	0.00	2.00	0.01	1.93	0.08	1.81	0.18
	$1B_{2u}$	2.22		2.73		2.11		2.12		2.01		2.01		1.99	
H_2Nc	$1B_{3u}$	2.08	−0.16	2.31	0.12	1.52	0.14	1.85	−0.10	1.68	−0.08	1.78	−0.04	1.56	0.03
	$1B_{2u}$	1.92		2.43		1.66		1.75		1.60		1.74		1.59	
H_2Ac	$1B_{3u}$	1.95	−0.22	2.17	0.06	1.26	0.04	1.65	−0.17	1.42	−0.15	1.68	−0.11	1.42	0.03
	$1B_{2u}$	1.73		2.23		1.30		1.48		1.27		1.57		1.45	
MAE[c]		0.41	0.15	0.76	0.09	0.12	0.12	0.24	0.13	0.13	0.12	0.15	0.06		

[a]Excitation energy in eV.
[b]Excitation energy difference in eV: $\Delta E = E(1B_{2u}) - E(1B_{3u})$.
[c]Mean absolute error from the experimental value.

TABLE VIII. Comparison of the excitation energies of Q-bands states with other works.

		SAC-CI[a]		TDDFT PBE0[b]		CASSCF[c]		CASPT2[d]		DFT/MRCI[e]		Exp.	
		EE	ΔE	EE	ΔE	EE	ΔE	EE	ΔE	EE	ΔE	EE	ΔE
H_2TAP	$1B_{3u}$	2.06	0.53							2.10	0.36	2.01	0.26
	$1B_{2u}$	2.59								2.46		2.27	
H_2Pc	$1B_{3u}$	1.83	0.28	2.10	0.02	3.56	−0.07	1.61	0.38	2.12	0.04	1.81	0.18
	$1B_{2u}$	2.11		2.12		3.49		1.99		2.16		1.99	
H_2Nc	$1B_{3u}$	1.52	0.14	1.84	−0.07							1.56	0.03
	$1B_{2u}$	1.66		1.77								1.59	
H_2Ac	$1B_{3u}$	1.26	0.04	1.65	−0.16							1.42	0.03
	$1B_{2u}$	1.30		1.49								1.45	

[a]SAC-CI/D95 this work.
[b]TDDFT PBE0/TZVP from Ref. 19.
[c]CASSCF(4,4)/6-31G calculation from Ref. 36.
[d]CASPT2(4,4)/6-31G calculation from Ref. 36.
[e]DFT/MRCI/DZP from Ref. 37.

also performed pure DFT, BLYP calculations. The calculated excitation energies were about 0.1–0.2 eV lower than those of the B3LYP calculations. For the splitting of the Q-bands, the trend was basically the same as with the B3LYP results. Our results agreed with the previous DFT study in which PBE0 functions with the TZVP basis were used.[19]

The importance of the LC for TDDFT has been shown in the application to large π-systems;[21] therefore, we performed the TDDFT calculation with the LC-BLYP functional. The LC decreased the excitation energies of H_2TAP and increased the excitation energies of H_2Nc and H_2Ac. The correction with H_2Pc was very small. Consequently, the LC-BLYP calculation well reproduced experimental excitation energies of H_2TAP. For H_2Pc, the LC-BLYP calculation agreed well with the experiment, even though the value of the splitting of the Q-bands was underestimated. For H_2Nc and H_2Ac, the LC-BLYP calculations tended to overestimate the excitation energies in comparison with H_2TAP and H_2Pc. The size of the splitting in the Q-bands for H_2Ac was larger than that for H_2Pc. From this behavior, we may conclude that LC-BLYP cannot reproduce the experimental trend for the splitting in the Q-bands, although the LC significantly improves the excitation energies.

The mean absolute errors (MAEs) from the experimental value are shown in Table VII. Although the energy order of the B_{3u} and B_{2u} states for H_2Nc and H_2Ac is different between the TDDFT and wave function methods, we simply assigned the calculated lower energy state to the observed lower energy one to calculate MAEs. The MAE of excitation energies by the SAC-CI calculations is smaller than the other methods, but the MAE of the energy differences is not so small mainly due to the error from H_2TAP.

Only a limited number of *ab initio* calculations have been reported on this series of molecules. There are only the PBE0/TZVP calculations for H_2Nc and H_2Ac.[19] CASSCF,[36] CASPT2,[36] and DFT/MRCI (Ref. 37) calculations have been reported for H_2Pc. These results are summarized in Table VIII. The PBE0/TZVP results are similar to our B3LYP/D95 results; therefore, the functional and basis set dependences would be minor for the excitation energies of the Q-bands. The CASSCF and CASPT2 results support the importance of dynamic electron correlation. The absolute excitation energies by CASSCF overshot the experimental values because of the very small active-space. The energy differences between the B_{2u} and B_{3u} states were similar to the CIS result. The energy difference was significantly improved by including dynamic electron correlation by PT2. Consequently, we conclude that dynamic electron correlation in excited states is essential for a proper description of the splitting of the Q-bands and the difference between the B_{2u} and B_{3u} states. That seems to be not completely considered by TDDFT. We also note that the many-body perturbation scheme, the so-called GW/BSE method, improved the TDDFT calculation of the splitting in the Q-bands of free-base porphin.[38] This result supports our findings. What we have to consider for correcting this discrepancy in TDDFT is still unclear, but correlated wave function methods for excited states, such as the SAC-CI and CIS(D), will be helpful for the investigating this problem.

Finally we discuss solvent effects. The experimental spectra of Fig. 4 were measured in pyridine. The deprotonation tendency in solution would reduce the Q-band splitting of free-base compounds. The vapor phase spectrum is available only for H_2Pc and the solvent effect decreases the Q-band splitting of H_2Pc. The spectrum of H_2Pc in THF solution has been reported in Ref. 15. The excitation energies in THF and in pyridine are almost the same. Freyer *et al.* studied the solvent effects on several free-base tetraazaporphyrines.[39] They noted that the solvent influences the splitting behavior in comparison with the gas phase spectra; however, the influence of solvent polarity on the Q-band splitting is small. Indeed, only single Q-band has been observed for H_2Nc in benzene.[39] The feature that the splitting of Q-bands decreases with increasing molecular size would be intrinsic for these molecules and would not be influenced by solvent effect.

VII. CONCLUSIONS

In this paper, we studied the excited states and UV-vis spectra of H_2TAP, H_2Pc, H_2Nc, and H_2Ac using the SAC-CI method. We calculated the states in the Q- and B-band re-

gions for excitation energies less than 4.5 eV. We calculated not only optically allowed states but also optically forbidden states in that region. The results of the present SAC-CI calculations consistently assigned the peaks observed by UV-vis and MCD spectroscopy to the optically allowed $\pi \rightarrow \pi^*$ transitions. The deviations between the calculations and experiment were about 0.3–0.4 eV when using the double-zeta basis sets. The results of SAC-CI calculations can be improved by using better basis sets and the present discussion and conclusion are limited within the double-zeta basis level.

The correlations of excited states between these four compounds were studied. The excited states corresponding to the Q-bands shift to lower energy with extension of the molecular size; while the excitation energies of the B-band states did not significantly depend on the molecular size. Such trends agree well with the experimental findings. In the larger molecules, transitions between other than the four-orbitals were obtained in the lower energy region. For H_2Ac, in particular, several states were calculated between the Q- and B-bands. The corresponding peaks have been observed by UV-vis and MCD spectroscopy.

The excitation energies of the Q-bands become smaller in accordance with the extension of the molecular size. This trend can be explained by the orbital energy levels of the HOMO. The degree of the Q-band shifts is suppressed for larger molecules. The findings are also explained by the orbital energies.

For free-base compounds, split Q-bands are observed because of the reduction from D_{4h} symmetry. For these TAP derivatives, the splitting of the Q-bands decreases with the extension of molecular size. This trend could be reproduced by the SAC-CI calculations; however, orbital energy levels could not explain this phenomenon. The CIS calculation did not agree with the observed trend of the splitting of the Q-bands. This trend could be explained by considering dynamic electron correlation by the CIS(D) or SAC-CI methods. The present results show the importance of electron correlation in excited states for an appropriate description of the Q-bands, or the difference between the B_{2u} and B_{3u} states of free-base compounds.

Standard TDDFT calculations could not reproduce this trend of the splitting of the Q-bands. The TDDFT results were similar to the CIS results. The long-range correction significantly improved the excitation energies of the Q-bands of these compounds; however, the effect was not enough to reproduce the experimental trend of the splitting of the Q-bands.

ACKNOWLEDGMENTS

H.N. acknowledges Professor N. Kobayashi for illuminating discussions on the natures of the excited states of large porphyrins and tetraazaporphyrins. The authors acknowledge support from a Grant-in-Aid for Scientific Research from the Japan Society for the Promotion of Science, the Next Generation Supercomputing Project. The computations were performed using the Research Center for Computational Science, Okazaki Research Facilities, NINS.

[1] Y. Rio, M. S. Rodríguez-Morgade, and T. Torres, Org. Biomol. Chem. **6**, 1877 (2008).
[2] T. Fukuda and N. Kobayashi, Dalton Trans. **2008**, 5685
[3] K. Toyota, J. Hasegawa, and H. Nakatsuji, Chem. Phys. Lett. **250**, 437 (1996).
[4] M. Gouterman, J. Mol. Spectrosc. **6**, 138 (1961); M. Gouterman, G. H. Wagnière, and L. C. Snyder, *ibid.* **11**, 108 (1963).
[5] H. Nakatsuji, J. Hasegawa, and M. Hada, J. Chem. Phys. **104**, 2321 (1996); Y. Tokita, J. Hasegawa, and H. Nakatsuji, J. Phys. Chem. A **102**, 1843 (1998).
[6] S. R. Gwaltney and R. J. Bartlett, J. Chem. Phys. **108**, 6790 (1998).
[7] L. Serrano-Andrés, M. Merchán, M. Rubio, and B. O. Roos, Chem. Phys. Lett. **295**, 195 (1998).
[8] T. Hashimoto, Y.-K. Choe, H. Nakano, and K. Hirao, J. Phys. Chem. A **103**, 1894 (1999).
[9] Z.-L. Cai, K. Sendt, and J. R. Reimers, J. Chem. Phys. **117**, 5543 (2002); Z.-L. Cai, M. J. Crossley, J. R. Reimers, R. Kobayashi, and R. D. Amos, J. Phys. Chem. B **110**, 15624 (2006).
[10] K. Toyota, J. Hasegawa, and H. Nakatsuji, J. Phys. Chem. **101**, 446 (1997).
[11] H. Nakatsuji and K. Hirao, J. Chem. Phys. **68**, 2053 (1978); H. Nakatsuji, Chem. Phys. Lett. **59**, 362 (1978); **67**, 329 (1979); **67**, 334 (1979).
[12] H. Nakatsuji, T. Miyahara, and R. Fukuda, J. Chem. Phys. **126**, 084104 (2007).
[13] H. Nakatsuji, Chem. Phys. **75**, 425 (1983); H. Nakatsuji, J. Hasegawa, and M. Hada, J. Chem. Phys. **104**, 232 (1996).
[14] J. Hasegawa, T. Kimura, and H. Nakatsuji, J. Porphyr. Phthalocyanines **9**, 305 (2005).
[15] N. Kobayashi, H. Ogata, N. Nonaka, and E. A. Luk'yanets, Chem.-Eur. J. **9**, 5123 (2003).
[16] N. Kobayashi, S. Nakajima, H. Ogata, and T. Fukuda, Chem.-Eur. J. **10**, 6294 (2004).
[17] K. Ishii, H. Itoya, H. Miwa, M. Fujitsuka, O. Ito, and N. Kobayashi, J. Phys. Chem. A **109**, 5781 (2005).
[18] J. Mack, Y. Asano, N. Kobayashi, and M. J. Stillman, J. Am. Chem. Soc. **127**, 17697 (2005).
[19] I. Lanzo, N. Russo, and E. Sicillia, J. Phys. Chem. B **112**, 4123 (2008).
[20] J. Hasegawa, K. Takata, T. Miyahara, S. Neya, M. J. Frisch, and H. Nakatsuji, J. Phys. Chem. A **109**, 3187 (2005).
[21] H. Iikura, T. Tsuneda, T. Yanai, and K. Hirao, J. Chem. Phys. **115**, 3540 (2001); M. Kamiya, H. Sekino, T. Tsuneda, and K. Hirao, *ibid.* **122**, 234111 (2005).
[22] C. Lee, W. Yang, and R. G. Parr, Phys. Rev. B **37**, 785 (1988); A. D. Becke, J. Chem. Phys. **98**, 5648 (1993).
[23] R. Ditchfield, W. J. Hehre, and J. A. Pople, J. Chem. Phys. **54**, 724 (1971); W. J. Hehre, R. Ditchfield, and J. A. Pople, *ibid.* **56**, 2257 (1972); P. C. Hariharan and J. A. Pople, Theor. Chim. Acta **28**, 213 (1973); M. M. Francl, W. J. Pietro, W. J. Hehre, J. S. Binkley, D. J. DeFrees, J. A. Pople, and M. S. Gordon, J. Chem. Phys. **77**, 3654 (1982).
[24] R. Fukuda and H. Nakatsuji, J. Chem. Phys. **128**, 094105 (2008).
[25] M. J. Frisch, G. W. Trucks, H. B. Schlegel *et al.*, GAUSSIAN development version, Revision H.01, Gaussian Inc., Wallingford, CT, 2009.
[26] T. H. Dunning, Jr., and P. J. Hay, in *Modern Theoretical Chemistry*, edited by H. F. Schaefer III (Plenum, New York, 1977), Vol. 3, pp. 1–27.
[27] B. Saha, M. Ehara, and H. Nakatsuji, J. Chem. Phys. **125**, 014316 (2006).
[28] Y. Kawashima, T. Hashimoto, H. Nakano, and K. Hirao, Theor. Chem. Acc. **102**, 49 (1999).
[29] V. I. Klimov, J. Phys. Chem. B **110**, 16827 (2006); I. Paci, J. C. Johnson, X. Chen, G. Rana, D. Popović, D. E. David, A. J. Nozik, M. A. Ratner, and J. Michl, J. Am. Chem. Soc. **128**, 16546 (2006).
[30] M. Head-Gordon, R. J. Rico, M. Oumi, and T. J. Lee, Chem. Phys. Lett. **219**, 21 (1994).
[31] M. J. Frisch, G. W. Trucks, H. B. Schlegel *et al.*, GAUSSIAN 09, Revision A.02, Gaussian Inc., Wallingford, CT, 2009.
[32] M. W. Schmidt, K. K. Baldridge, J. A. Boatz, S. T. Elbert, M. S. Gordon, J. H. Jensen, S. Koseki, N. Matsunaga, K. A. Nguyen, S. J. Su, T. L. Windus, M. Dupuis, and J. A. Montgomery, J. Comput. Chem. **14**, 1347 (1993).
[33] R. P. Linstead and M. Whalley, J. Chem. Soc. **1952**, 4839.
[34] L. Edwards and M. Gouterman, J. Mol. Spectrosc. **33**, 292 (1970).
[35] P. Liljeroth, J. Repp, and G. Meyer, Science **317**, 1203 (2007).

[36] H. Cortina, M. L. Senent, and Y. G. Smeyers, J. Phys. Chem. A **107**, 8968 (2003).
[37] A. B. J. Parusel and S. Grimme, J. Porphyr. Phthalocyanines **5**, 225 (2001).
[38] M. Palummo, C. Hogan, F. Sottile, P. Bagalá, and A. Rubio, J. Chem. Phys. **131**, 084102 (2009).
[39] W. Freyer, S. Muller, and K. Teuchner, J. Photochem. Photobiol., A **163**, 231 (2004).